Doping Behavior of Implanted Magnesium in Silicon

H. Sigmund and D. Weiß

Fraunhofer-Institut für Festkörpertechnologie, Paul-Gerhardt-Allee 42, D-8000 München 60, Fed. Rep. of Germany

Abstract

Mg-implanted layers (5×10^{14} to 5×10^{15} cm^{-2}) which are annealed at low temperatures (500°C to 600°C) show high n-type conductivity. Contrary to the usual doping elements in silicon, the sheet carrier concentration shows a sharp decrease with increasing annealing temperatures; minimum sheet resistivities of 800 $\Omega/\square$ were obtained after a "thermal" annealing step at 550°C for 30 min. From profile measurements (Hall effect and SIMS), it is concluded that the interstitial solubility for Mg at 500°C in these samples is as high as 1×10^{18} cm^{-3}. At temperatures above 700°C the electrically active Mg concentration is rapidly gettered by the damage layer and Mg precipitates, and becomes electrically inactive. A model for the segregation behavior of Mg in silicon is discussed briefly.

1. Introduction

It is known, based on absorption and ESR measurements made on Mg-diffused silicon samples, that interstitially dissolved Mg in silicon forms a double donor with the donor levels E_{D1} = 0.11 eV and E_{D2} = 0.25 eV [1,2]. The preparation of these samples was accomplished by sandwich diffusion at 1200°C. The samples showed a very low interstitial solubility ($\approx 10^{15}$ cm^{-3}), as revealed by resistivity measurements [1]. Measurements of the totally dissolved Mg were not made in these experiments. Recently performed investigations on the segregation and solubility of Mg in silicon at high temperatures (950°C to 1200°C), by atomic-absorption spectroscopy (AAS) as well as by secondary-ion mass spectroscopy (SIMS), have revealed a high solubility of Mg (4×10^{18} to 1.5×10^{19} cm^{-3}) [3]. The samples were prepared by special liquid-phase epitaxy; the epi-layers showed conductivity values similar to the diffused samples. In order to investigate the segregation and doping behavior of Mg in silicon at lower temperatures, these experiments with implanted Mg were performed. The isothermal annealing and diffusion behavior in the temperature range between 450°C and 950°C was investigated through SIMS and Hall-effect measurements.

2. Experimental Procedure

Samples with patterns of the van-der-Pauw type [4] were made using the planar technique (Fig. 1). An important aspect of the van-der-Pauw structure is represented by the As-implanted contacts, which ensure ohmic beha-

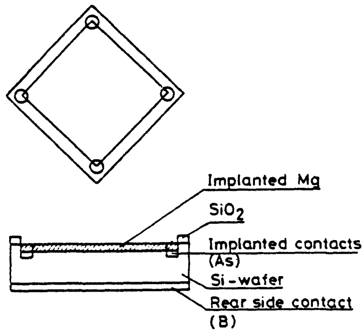

Fig. 1. Van-der-Pauw pattern

Fig. 2. Theoretical (continous line) and measured (SIMS) Mg distribution of a 150 keV implantation. It can be seen that the Mg penetrates more deeply into the crystal than would be expected from the gaussian distribution with R_p and ΔR_p values according to Biersack [9] ►

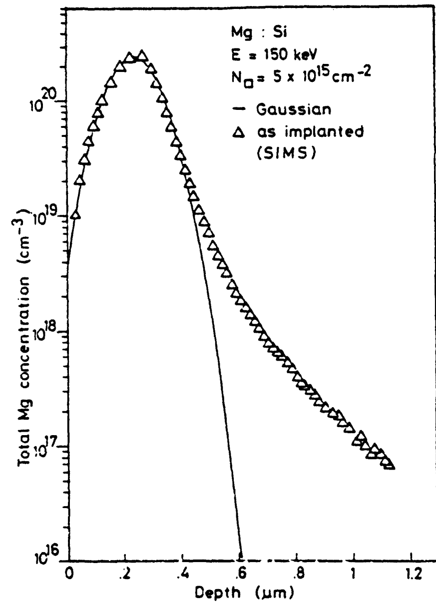

vior even at high annealing temperatures. Boron implantation into the back surface (unpolished) improved the contact on the reverse side, which is useful for the anodic stripping technique and measurement of current-voltage characteristics. The implanted contacts were annealed for 30 min at 900°C. Samples prepared in this manner were implanted with Mg into the polished surface at room temperature. Data on starting material and the implantation parameters are listed in Table 1. To avoid channeling, the angle of incidence was 7° relative to the (111) crystal direction. Figure 2 shows the theoretical and measured (SIMS) distribution of a 150 keV Mg implantation into Si. A dose of 5×10^{15} cm^{-2} is assumed to reach the amorphous dose, while 5×10^{14} cm^{-2} is below this dose [5]. After implantation, the slices were cut into quadratic wafers containing one van-der-Pauw pattern each (Fig. 1). Isothermal annealing between 400°C and 800°C was carried out in a nitrogen atmosphere. Time intervals from 7.5 to 90 min were used; continous 6 h isothermal annealing was applied to some samples. The effective carrier density $N_{S,eff}$ and the effective mobility μ_{eff} is given by $N_{S,eff} = r/(e \cdot R_{H,S})$ and $\mu_{eff} = R_{H,S}/(r \cdot \rho_S)$, where $R_{H,S}$ is the measured sheet Hall coefficient and ρ_S the sheet resistivity. Following the usual practice, the scattering factor r is approximated by unity. Interpretation of the effective values are discussed in detail by Baron et al. [6]. The measurements were carried out at room temperature. To avoid errors due to magnetoelectric effects (Nernst, Ettinghausen, Righi-Leduc, etc.), current and voltage probes were cyclically exchanged [7]. Therefo-

Table 1: Material and implantation data

Si wafers, Wacker Fz-Si	Doses 5×10^{14} and $5 \times 10^{15} cm^{-2}$
Orientation (111)	Energy 80 and 150 keV
Resistivity 50 Ωcm, p-type	R_p 0.139 and 0.238 μm
one side polished	ΔR_p 0.053 and 0.0829 μm

re, ρ_S and $R_{H,S}$ are average values extracted from these current and voltage measurements. Anodic stripping technique [8] was used for determination of the number of carriers as a function of depth. The applied electrolyte was NMA (0.025g KNO_3 dissolved in 10 ml H_2O + 500 ml N-methylacetamide); the forming voltage was 120 V. The thickness of the removed layer was determined mechanically, the average of one step was 26 ± 2nm.

3. Experimental Results

The isothermal annealing experiments showed that Mg-implanted samples display a quite different doping behavior than that for implantation with the ordinary doping elements. The results are shown in Fig. 3, where the effective carrier density $N_{S,eff}$ is plotted against the annealing time. All samples with a dose of 5×10^{15} cm^{-2} showed a decreasing sheet carrier concentration with increasing annealing time (> 7.5 min), until they reached a nearly constant value for a certain temperature. In samples with a dose of 5×10^{14} cm^{-2}, the sheet carrier concentration at low temperatures (500°C, 550°C) first increases, then reaches a maximum, and finally drops to nearly the same value as in the amorphous sample. Figure 3 shows that a temperature-dependent, quasi-equilibrium sheet carrier concentration is established, the level of which drops drastically with increasing annealing time. A good example of this characteristic is represented by the 600°C isothermal curves, where the equilibrium $N_{S,eff}$ value is reached after annealing for ca. 3 h. The 800°C isotherms show a nearly constant sheet carrier density value over the whole investigated range - the $N_{S,eff}$ decrease obviously occurs so quickly that it cannot be observed in these

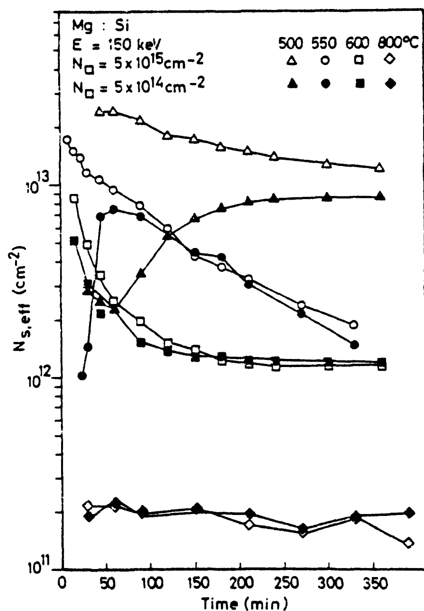

Fig. 3. Isothermal annealing curves for four different temperatures

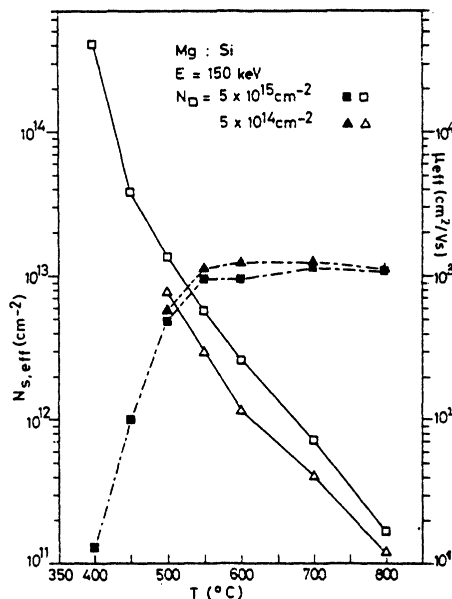

Fig. 4. Effective carrier concentration ($N_{S,eff}$) and effective mobility (μ_{eff}) after 6 h isothermal annealing

measurements. The non-constant behavior of the 550°C isotherms is assumed to result from a measurement error due to non-ohmic contacts, which can cause $N_{S,eff}$ values which are to low. Figure 4 shows the effective carrier density $N_{S,eff}$ and the effective mobility versus annealing temperature after 6 h isothermal annealing for a temperature range from 400°C up to 800°C. Samples implanted with a dose of 5 x 10^{15} cm^{-2} could only be measured at an annealing temperature of 500°C and above, due to poor recrystallization at lower temperatures. Implants with 5 x 10^{15} cm^{-2} already showed a high effective sheet carrier density (about 10% electrically active) at an annealing temperature of 400°C. Figure 5 shows current-voltage characteristics under reverse bias, whereby the annealing temperatures are the variable parameter. The plotted curves show a steep reduction of leakage current between 450°C and 500°C annealing temperature, while at higher annealing temperatures the drop occurs much more gradually. The temperature range from 400°C up to 550°C is characterized by a steep increase in the effective mobilities μ_{eff}, due to the recrystallization with increasing annealing temperature in this range. At temperatures higher than 550°C, the mobility values are almost in agreement with Irvin's data [10]. Mobilities in layers with a dose of 5 x 10^{15} cm^{-2} lie below the values of samples implanted with a dose of 5 x 10^{14} cm^{-2}. The effective sheet carrier concentrations decrease almost exponentially over the entire investigated range. The measured $N_{S,eff}$ value is only slightly dependent on the implantation dose. It should be mentioned that in our experiments the effective carrier density is not reversible. This means that an established value of $N_{S,eff}$ for an annealed sample cannot be increased again by annealing it at a lower temperature.

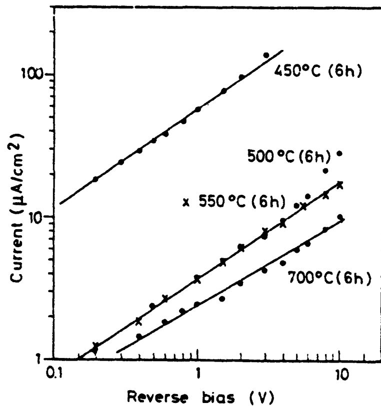

Fig. 5. Reverse current-voltage characteristics for different annealing temperatures (dose: 5 x 10^{15} cm^{-3}, 150 keV)

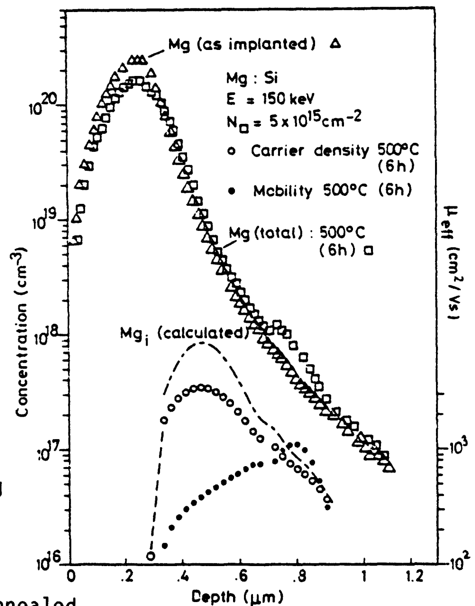

Fig. 6. Doping profiles and mobilities (μ_{eff}) of a sample isothermal annealed. Shown is the total Mg distribution (SIMS) and the measured carrier distribution (at room temperature) in comparison to the calculated interstitial concentration of Mg.

Distributions of carriers, determined by Hall-effect and sheet-resistitivity measurements combined with anodic stripping, are compared to SIMS profiles. With the SIMS technique the total amount of Mg in the sample can be determined. In Fig. 6, the total Mg distribution in a sample - implanted with a dose of 5×10^{15} cm^{-2} (150 keV) - before and after a 6 h annealing at 500°C is plotted. An important finding is that after annealing the Mg remains in the sample to a large extent (75%). The other 25% of the Mg is assumed to be at the surface probably as MgO. The small peak at a concentration of 1.5×10^{15} cm^{-2} suggests a slight diffusion into the crystal. Figure 6 also shows the number of carriers and the mobility as a function of depth. All data were obtained after 6 h annealing at 500°C. It is seen clearly that only a small percentage of the total Mg atoms is electrically active. Brooks [11] has shown that the average number (f) of electrons occupying a double donor is given by:

$$f = \frac{2}{1+[1+4\exp(E_{D2}-E_F)/kT]/1+4\exp(E_F-E_{D1})/kT]} , \qquad (1)$$

where E_{D1} and E_{D2} are the first and second donor levels, respectively. The Fermi level E_F can be obtained (if E_F is several kT below the bottom edge of the conduction band E_c) from $n \cong N_c \exp((E_F-E_c)/kT)$ with N_c being the effective density of states in the conduction band. Thus, the concentration of Mg interstitials (Mg_i) can be calculated from Eq (1) and the expression: $Mg_i = n/(2-f)$. In Fig. 7, the average number of electrons per Mg_i atom transferred to the conduction band is plotted versus the Mg_i concentration for several temperatures. It should be noted that temperature-dependent Hall-effect and sheet-resistivity measurements indicate increasing carrier densitiy with increasing temperature (Fig. 8).

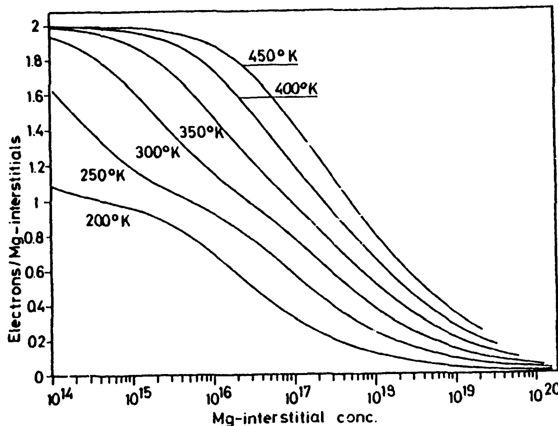

Fig. 7. Probability of ionization of interstitial Mg in dependence of the Mg doping level

The concentration of interstitial Mg atoms, determined by Eq. (1) from the measured electron density is plotted in Fig. 6 (dashed line). The total Mg concentration is greater than the interstitial concentration by factor of 6 in the tail and by a factor of 17 at the maximum of the Mg - interstitial distribution. The ratio increases sharply as one comes closer to the surface. The carrier profile could only be determined at a depth of 0.25 µm and above, where the concentration increases rapidly. Increase of the

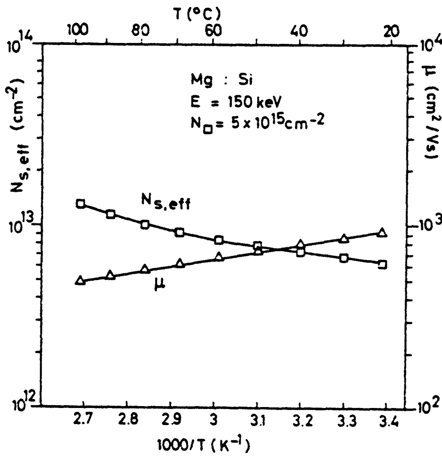

Fig. 8. Temperature dependence of the effective carrier concentration ($N_{S,eff}$) and mobility (μ_{eff}) (550°C, 6 h)

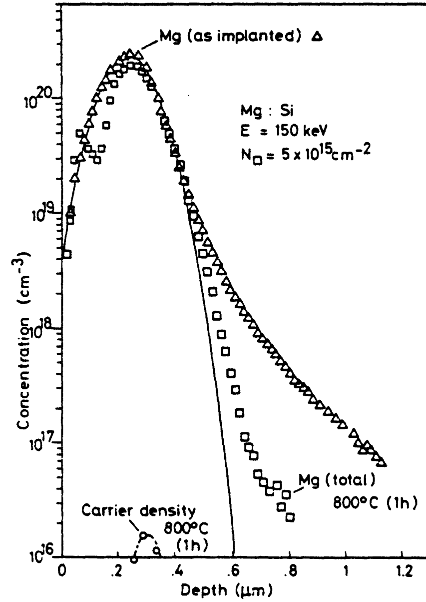

Fig. 9. Doping profile of Mg (SIMS) as implanted and after isothermal annealing (800°C, 1h); also shown is the measured peak of the carrier profile

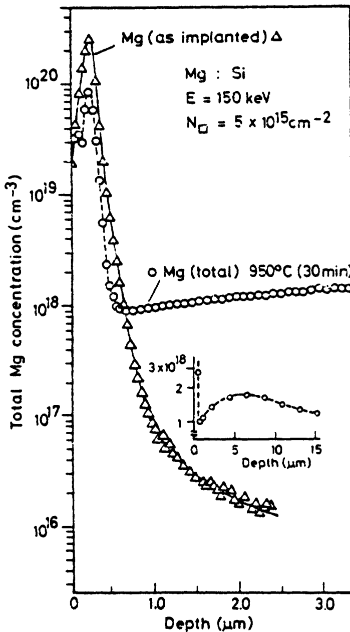

Fig. 10. Doping profile (SIMS) of Mg after an isothermal annealing at 950°C, 30 min.

carrier concentration is accompanied by increasing mobilities. In Fig.9 the total Mg concentration and measured electron concentration after 1 h annealing at 800°C is shown. Also in this case, 75% of the implanted Mg remains in the sample. At this annealing temperature, Mg does not diffuse into the crystal, but approaches the Gaussian implantation distribution. It can therefore be concluded that the Mg is gettered by the

damage region or by Mg precipitates. This peak in carrier concentration lies closer to the surface (0.29 µm) than the maximum of the carrier distribution after a 6h annealing at 500°C. This suggests that the damage layer becomes thinner and that the crystal recrystallizes from the bulk. The maximum of the electron density now has a value of about 2×10^{16} cm^{-3}. An interesting phenomenon is observed when the annealing temperature is increased to 950°C. Figure 10 shows SIMS profiles before and after a 30 min annealing at 950°C, a temperature which lies slightly above the eutectic point. Mg diffuses fast into the crystal at a concentration of about 2×10^{18} cm^{-3}, and could be measured even at a depth of 15 µm. Hall measurements on samples annealed at temperatures higher than 800°C could not be performed.

4. Discussion

In order to explain the annealing and doping behavior of implanted Mg in silicon, the following segregation model is proposed. According to this model, the implanted depth is divided into two regions (A and B) as depicted in Fig. 11. Region A can be characterized by low carrier concentration ($\approx 5 \times 10^{15}$ cm^{-3}) low Hall mobilities, whereas the total Mg concentration in this region is several orders of magnitude above the measured electron concentration. Region B shows high electron concentrations with high mobility values (close to bulk mobilities); a high fraction of the total Mg concentration is electrically active. Because substitutional Mg (Mg_s) in silicon probably forms a deep acceptor level (preliminary DLTS measurements have revealed a level at 0.55 eV), a strong compensation should occur if the number of substitutional Mg atoms exceeds the concentration of interstitial Mg atoms. The implanted samples showed n-type conductivity in all cases. It is therefore very likely that at lower annealing temperatures, Mg_i atoms react with Mg_s atoms and form neutral complexes: $Mg_i + Mg_s = (Mg_s \cdot Mg_i)$.

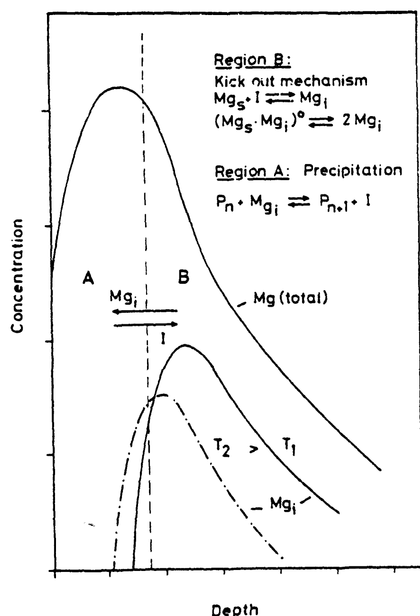

Fig. 11. Model for the annealing behavior of implanted Mg in silicon

The complexes ($Mg_s \cdot Mg_i$) are isoelectronic, so they should have no influence on the electron concentration. At higher temperatures, the complexes in region B dissociate. Furthermore, the substitutional Mg atoms react with Si interstitials (I) according to the "Kick-out" mechanism [12]: $Mg_s + I = Mg_i$. The total reaction between Si interstitials and the complexes would then be:

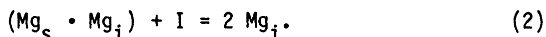

$$(Mg_s \cdot Mg_i) + I = 2\ Mg_i. \qquad (2)$$

Between regions A and B, there is a sharp gradient in the interstitial Mg concentration (s. Fig. 11). This concentration gradient is much steeper then the gradient into the bulk. Thus, at higher temperatures, Mg_i atoms diffuse rapidly into region A, and the Mg concentration is increased . It seems very probable that Mg silicide clusters are formed in region A. A suitable reaction may be given in the following form: $P_n + Mg_i = P_{n+1} + I$, where P_n is a Mg-silicide precipitation with n Mg atoms. Based on this assumption, the experimentally observed annealing kinetics of Fig. 3 may be described analytically [3]. At temperatures between 900°C and 950°C, the equilibrium point of the precipitation reaction is shifted to the left side of Eq.(2), and Mg atoms diffuse into the bulk rapidly. This drastic change in the behavior of region A occurs in a very small temperature interval, so that is very probable that the structure of the precipitates is changed between 900°C and 950°C.

We are indebted to Mr. Kranz/IFT for performing the implantation of the samples.

References

1. R.K. Franks, J.B. Robertson: Sol. State Comm. 5, 479 (1967)
2. L.T. Ho, A.K. Ramadas: Phys. Rev. 35, 462 (1972)
3. H. Sigmund, R. Braungart. Ch. Höpfl, D. Weiß: Research Report NT 846 (1981) FRG
4. L.J. van der Pauw: Philips Res. Repts. 13, 1 (1958)
5. H. Ryssel, I. Ruge: Ionenimplantation, Stuttgart (1978), p. 33
6. R. Baron, G.A. Shifrin, O.J. Marsh, J.W. Mayer: J. Appl. Phys. 40, 3702 (1969)
7. H.H. Wieder, Characterisation of Epitaxial Semiconductor Films, ed. by H. Kressel, N.Y. (1976)
8. A. Manara, A. Ostidich, G. Pedroli, G. Restelli: Thin Solid Films 8, 359 (1971)
9. J.P. Biersack: Hahn-Meitner-Report, HMI-B334 (1980): projected ranges of the most common ion-target combinations are published in [5].
10. S.M. Sze, J.C. Irvin: Solid-State Electronics 11, 599 (1968)
11. H. Brooks: Advances in Electronics and Electron Physics, Vol 7. N.Y. (1955)
12. A. Seeger: phys. stat. sol.(a) 61, 521 (1980)